NEOPLASIA
www.neoplasia.com

Volume 11 Number 1 January 2009 pp. 48–56 48

Evaluation of Angiogenesis Using Micro–Computed Tomography in a Xenograft Mouse Model of Lung Cancer

Rajkumar Savai*, Alexander Claus Langheinrich†, Ralph Theo Schermuly‡,§, Soni Savai Pullamsetti‡,§, Rio Dumitrascu‡, Horst Traupe¶, Wigbert Stephan Rau†, Werner Seeger‡,§, Friedrich Grimminger*,‡ and Gamal Andre Banat*

*Department of Hematology and Oncology, Justus-Liebig-University, Klinik Strasse 36, 35385 Giessen, Germany; †Department of Radiology, Justus-Liebig-University, Klinik Strasse 36, Giessen, 35385 Germany; ‡Department of Internal Medicine, Justus-Liebig-University, Klinik Strasse 36, 35385 Giessen, Germany; §Department of Lung Development and Remodelling, Max-Planck-Institute for Heart and Lung Research, Parkstrasse 1, 61231 Bad Nauheim, Germany; ¶Department of Neuroradiology, Justus-Liebig-University, Klinik Strasse 36, 35385 Giessen, Germany

Abstract

Quantitative evaluation of lung tumor angiogenesis using immunohistochemical techniques has been limited by difficulties in generating reproducible data. To analyze intrapulmonary tumor angiogenesis, we used high-resolution micro–computed tomography (micro-CT) of lung tumors of mice inoculated with mouse Lewis lung carcinoma (LLC1) or human adenocarcinoma (A549) cell lines. The lung vasculature was filled with the radiopaque silicone rubber, Microfil, through the jugular vein (*in vivo* application) or pulmonary artery (*ex vivo* application). In addition, human adenocarcinoma lung tumor–bearing mice treated site-specifically with humanized monoclonal antibody (bevacizumab) against vascular endothelial growth factor. Quantitative analysis of lung tumor microvessels imaged with micro-CT showed that more vessels (mainly small, <0.02 mm^2) were filled using the *in vivo* (5.4%) compared with the *ex vivo* (2.1%) method. Furthermore, bevacizumab-treated lung tumor–bearing mice showed significantly reduced lung tumor volume and lung tumor angiogenesis compared with untreated mice as assessed by micro-CT. Interestingly, microvascularization of mainly the smaller vessels (<0.02 mm^2) was reduced after bevacizumab treatment. This observation with micro-CT was nicely correlated with immunohistochemical measurement of microvessels. Therefore, micro-CT is a novel method for investigating lung tumor angiogenesis, and this might be considered as an additional complementary tool for precise quantification of angiogenesis.

Neoplasia (2009) 11, 48–56

Introduction

Lung cancer affects a greater number of people worldwide than any other cancer and is the leading cause of cancer death (~28%) in both men and women. The global incidence of this disease is rising by ~0.5% per year, and the number of cancer deaths caused by lung cancer expected to increase to 50% by 2020 [1]. Because lung cancer patients are typically diagnosed at a late stage, prognosis for most patients remains poor, with a 5-year survival rate of less than 15%. The current situation highlights the fact that lung cancer treatment requires new approaches, and recent research has focused on molecular-targeted therapies [2].

Angiogenesis, the process of new blood vessel formation, is fundamental for the growth and spread of solid tumors. Generally, tumors

Abbreviations: micro-CT, micro–computed tomography; LLC1, Lewis lung carcinoma; MIP, maximum intensity projection; VRT, volume rendering technique; VEGF, vascular endothelial growth factor

Address all correspondence to: Gamal Andre Banat, MD, PhD, MBA, and Rajkumar Savai, PhD, Department of Hematology and Oncology, Justus-Liebig-University, Klinikstrasse. 36, D-35385 Giessen, Germany. E-mail: A.Banat@innere.med.uni-giessen.de; Savai.Rajkumar@innere.med.uni-giessen.de

Received 27 August 2008; Revised 5 October 2008; Accepted 7 October 2008

DOI 10.1593/neo.81036

cannot grow beyond 2 mm in diameter without developing a vascular supply [3]. Moreover, angiogenesis not only permits further growth of the primary tumor but also provides a means for metastatic dissemination. Molecular abnormalities such as alterations in the expression of vascular endothelial growth factor (VEGF), basic fibroblast growth factor, platelet-derived growth factor, transforming growth factor-β, granulocyte/monocyte colony-stimulating factor, angiostatin, and endostatin are responsible for this pathologic angiogenesis process [4,5]. Therefore, inhibition of specific molecules essential for the tumor vascular development has become a key therapeutic antitumor strategy. The most promising of these targets is the VEGF pathway, targeted either by preventing VEGF binding to its receptor or inhibiting signaling downstream from the receptor. The first drug to use this concept was bevacizumab (Avastin), a humanized antibody against VEGF, which was approved for lung cancer treatment worldwide in 2006/2007 [6,7].

Recent evidence suggests that angiogenesis in many solid tumors is a major factor in predicting the aggressiveness of the disease and patient survival in different tumor types, including lung cancer [8–12]. Specifically, high vascularity at the periphery of lung tumors has been correlated with tumor progression [13]. Tumor vascularization is usually quantified by determining microvessel density either histologically, by a visual count of blood vessels under high-magnification light microscopy, or immunohistochemically, by staining for endothelial antigens such as CD34, CD31 (PECAM), von Willebrand factor (vWF), factor VIII–related antigen, and VEGF [14].

The methods mentioned are relatively subjective, not truly quantitative, and two dimensional, and are thus not necessarily representative of vascularity throughout the entire sample. A recent meta-analysis of individual patient data from published and unpublished data sets did not demonstrate a prognostic value for microvessel density analysis in patients with nonmetastatic surgically treated non–small cell lung cancer [15]. Similarly, further studies in which the three-dimensional (3D) structure of tumor microvasculature was obtained mainly by analyzing histologic serial sections, and filling the blood vessels with an opaque substance also posed inherent problems, such as misalignment, missing sections, and imperfect perfusion [16–19]. Despite these difficulties, accurate quantification of tumor angiogenesis has recently been shown to be of potential significance. In this regard, dynamic contrast-enhanced computed tomography (CT), dynamic contrast-enhanced magnetic resonance imaging, flat-panel volumetric-CT (fpvCT), and micro–CT have emerged as promising technologies that can overcome several of the challenges associated with the evaluation of vascular networks [20,21]. Moreover, micro-CT offers the unique advantage of imaging a representative sample volume at high resolution (~5- to 10-μm isotropic voxels) without physically sectioning it and without limitations related to either the plane of the section, superimposition, or distortions frequently observed with histology. Furthermore, the 3D nature of the micro-CT data set allows calculations of vessel tortuosity, an index of angiogenesis. Indeed, this technique has been used to visualize the vasculature in intact isolated rodent organs [22] and the myocardial, renal, and hepatic vasculature [23–27] and trabecular bones [28] in surgical bone specimens. Although this technique allows serial imaging of vessel number and morphology in *ex vivo* specimens, which might be useful in the evaluation of angiogenesis and treatment options, to date, it has not been evaluated in detail in experimental models of lung cancer.

In parallel with the development of high-resolution imaging and quantification of angiogenesis of lung tumors, a need has arisen for the development of site-specific treatment strategies that are efficacious without the unacceptable systemic adverse effects of conventional treatments. Along these lines, we recently used a combination of microscopic analysis of infused fluorescent microspheres and 3D images obtained by micro-CT and fpvCT to show that the pulmonary arterial system plays a predominant role in the blood supply of orthotopic lung tumors in mice [29].

The purposes of our study were to (i) evaluate the feasibility of micro-CT for the quantification of lung tumor angiogenesis, (ii) correlate micro-CT data with histologic data, and (iii) quantify the antiangiogenic effect of site-specifically delivered bevacizumab in a mouse model of lung cancer.

Materials and Methods

Cell Lines and Culture Conditions

Mouse Lewis lung carcinoma (LLC1) and human A549 lung adenocarcinoma cell lines were obtained from American Type Culture Collection (Manassas, VA). LLC1 cells were maintained in RPMI-1640 medium supplemented with 2% fetal bovine serum, penicillin (100 U/ml), and streptomycin (0.1 mg/ml) at 37°C in a humidified atmosphere containing 5% CO_2. A549 cells were maintained in Dulbecco's modified Eagle's medium/F-12 medium supplemented with 10% fetal bovine serum, penicillin (100 U/ml), streptomycin (0.1 mg/ml), 1% minimum essential medium vitamin solution, 2 mM glutamate, and 1% nonessential amino acids at 37°C in a humidified atmosphere containing 5% CO_2 (all reagents were from Gibco, Germany).

Lung Tumor Xenograft Models

Female C57/BL6 (5-7 weeks old) and BALB/c *nu/nu* (7-8 weeks old) mice were purchased from Charles Rivers, Sulzfeld, Germany, kept under pathogen-free conditions, and handled in accordance with the University of Giessen recommendations for experimentation. The lung tumor models was generated by intratracheal instillation of 1×10^6 LLC1 cells into C57/BL6 mice and 2×10^6 A549 cells into BALB/c *nu/nu* mice as described [29,30]. For all the experiments (intratracheal instillation, treatment, and microfill injections), mice were anesthetized by intraperitoneal injection of a mixture containing ketamine (100 mg/ml; Ketavet; Pharmacia & Upjohn, Erlangen, Germany) and xylazine (2%; Rompun; Bayer, Leverkusen, Germany).

Treatment of Lung Tumor–Bearing Mice

After detecting lung tumors with fpvCT 5 to 6 weeks after tumor cell injection, human A549 adenocarcinoma tumor–bearing mice were anesthetized and implanted with osmotic minipumps (Model 2002; Alzet Corp., Palo Alto, CA) for continuous drug administration according to the manufacturer's instructions. Briefly, osmotic minipumps were filled with distilled water (200 μl per pump) or anti-VEGF antibody bevacizumab (Avastin; Roche, Welwyn Garden City, UK; dose, 5 mg/200 μl per pump) and were incubated in isotonic saline 24 hours at 37°C before implantation. *In vitro* testing showed that the minipumps reached a steady pumping rate in 24 hours. The pump was implanted intraperitoneally and connected to a jugular catheter that was introduced into the jugular vein under sterile conditions from a small midline incision. The incision was closed in two layers with polypropylene sutures [31]. These pumps (internal volume, 200 μl) continuously delivered bevacizumab at a rate of 0.5 μl/h for 14 days. To monitor the effects of bevacizumab on lung tumor growth, mice

were scanned with fpvCT. At the end of the treatment protocol, mice were anesthetized and injected with Microfil for micro-CT scannings.

Micro-CT

After confirming the presence of lung tumors in mice using fpvCT [29,30] (data not shown), blood vessels were filled with a solidifying silicone rubber blood pool contrast agent (Microfil; Flow Tech, Carver, MA) to form a vascular cast for investigations using micro-CT. Under visual control, ready-made nondiluted Microfil was manually perfused using two different methods as described [29,32]. Briefly, mice were infused with heparin and either (i) the lung vascular tree was completely filled by *in vivo* injection through the jugular vein or (ii) the pulmonary arteries were filled by direct injection of Microfil into the main pulmonary artery *ex vivo*. After perfusion and solidification of the contrast medium, the lungs were removed and scanned with a desktop micro-CT unit (Skyscan1072; Skyscan, Aartselaar, Belgium) as described [29,32]. Samples were positioned on a computer-controlled rotation stage and scanned 180° around the vertical axis in rotation steps of 0.675° at 60 kV. Acquisition time for each view was 2.4 seconds. Raw data were reconstructed with a modified Feldkamp cone-beam reconstruction algorithm, resulting in 8-bit grayscale images with 6- to 10-μm^3 isotropic voxels. Image processing, tissue density measurements, extraction of lung tumors, quantification of tumor vascularization, and tree analysis on tumor vascularization were performed with the Analyze 7.0 software package (Analyze; Biomedical Imaging Resource, Mayo Foundation, Rochester, MN). After treatment with bevacizumab in BALB/c *nu/nu* mice, lungs were monitored with fpvCT, and lung vasculature was filled *in vivo* as above for micro-CT investigation.

Immunohistochemistry

Lungs were harvested, and each lung lobe was embedded in paraffin blocks and sectioned at 3 μm. A total of 50 to 80 serial sections were made from each lung lobe tissue block. Sections were stained with hematoxylin and eosin and were analyzed using a light microscope (Leica Instruments, Nussloch, Germany) for the presence of the tumor mass for correlation with the micro-CT images.

After deparaffinization of the lung tumor sections, endogenous peroxidases were blocked with 0.3% (v/v) H_2O_2 in methanol and then blocked with 5% (v/v) bovine serum albumin in phosphate-buffered saline, followed by incubation with rabbit polyclonal anti-vWF (dilution 1:800; Dako, Hamburg, Germany) and rabbit polyclonal anti–proliferating cell nuclear antigen (PCNA, dilution 1:200; Santa Cruz Biotechnology, Santa Cruz, CA). Sections were washed in phosphate-buffered saline, and antibody binding was determined using an ImmPRESS reagent kit (Vector Laboratories, Burlingame, CA). After extensive washing, sections were stained with vector VIP and NovaRED (Vector Laboratories) and counterstained with nuclear fast red and hematoxylin (Vector Laboratories). The immunohistologic staining for vWF and PCNA was quantified in 10 different randomly chosen fields of lung tumor sections by light microscopy at a magnification of 100×.

Results

Analysis of micro-CT Images

In vivo injection of Microfil through the jugular vein and *ex vivo* injection of Microfil through the pulmonary artery both resulted in fixation of the pulmonary vascular tree with preservation of both microarchitecture and 3D interconnectivity of the entire lung (Figure 1). Both methods resulted in successful filling of the pulmonary arteries down to the level of the alveolar capillaries and a clear visualization of the pulmonary microcirculation to lung tissue and lung tumors (Figure 1). The high-resolution 3D renderings of the vascular tree micro-CT images of intrapulmonary tumors and their microvascularization images were generated with 3D maximum intensity projection (MIP) and 3D volume rendering technique (VRT). The 3D MIP images (Figure 1*A*) show the main anatomical lung features such as tumor mass, pulmonary arteries, pulmonary veins, trachea, mediasternum, and esophagus. The 3D VRT images (Figure 1*B*) show large and microvessels in the lung and microvessels (pulmonary arteries, pulmonary veins) distributed in the whole lung.

The micro-CT images were compared to the corresponding histologic images—the criterion standard for morphologic analysis—and the samples showed a high degree of agreement by visual assessment for both *in vivo* and *ex vivo* vessel filling (Figure 1*C*). Figure 1*D* shows a clear correlation between the two imaging techniques, and the anatomical structures of tumor masses, Microfil-filled vasculature, pulmonary arteries, and bronchoalveolar structures are observed in both the micro-CT and histology images.

Quantification of Lung Tumors and Lung Tumor Microvessels

After analyzing whole-lung images using *ex vivo* and *in vivo* vessel filling methods, the tumor masses were selected and virtually extracted from the lung images and tumor volume and tumor vessel volume were measured (Figure 2*A*). Interestingly, *in vivo*–filled tumors had more vessels perfused compared to *ex vivo*–filled tumors. With the *in vivo* filling method, the tumor volume was 2.93 ± 0.83 mm^3, and the perfused tumor vessel volume was 0.16 ± 0.03 mm^3, thus implying a 5.4 ± 0.4% vessel volume contribution to the total tumor volume (Figure 2*B*). The *ex vivo* filling method measured a 3.47 ± 1.00-mm^3 lung tumor volume and a 0.08 ± 0.03-mm^3 perfused tumor vessel volume, thus implying a 2.2 ± 0.32% vessel volume contribution to the total tumor volume (Figure 2*C*). These results nicely correlated with tumor microvessel quantification.

More microvessels (0.001-0.01 mm^2 in diameter) were filled in the *in vivo*–filled tumors compared to the *ex vivo*–filled tumors (2039 *vs* 1214, respectively). Similar differences between *in vivo* and *ex vivo* filling were also found in microvessels ranging from 0.051 to 0.06 mm^2 in diameter (27.4 *vs* 21.5, respectively), suggesting that more microvessels were perfused with the *in vivo* vessel filling method compared to the *ex vivo* filling method (Figure 3).

Quantitative Analysis of Angiogenesis with Site-Specific Therapy

To quantify the potential antiangiogenic effect of bevacizumab, after detecting lung tumors with fpvCT (data not shown), animals were treated with bevacizumab, and contrast-enhanced 3D MIP images from untreated and bevacizumab-treated mice were obtained after 14 days of treatment. As anticipated, bevacizumab treatment reduced tumor growth (Figure 4*A*). In addition, tumor angiogenesis in extracted tumors was significantly reduced in bevacizumab-treated animals compared to untreated animals (Figure 4*B*). Moreover, the mean survival rate increased with bevacizumab therapy (data not shown).

Quantification of tumor angiogenesis demonstrated a significant reduction of tumor size and tumor angiogenesis in the bevacizumab-treated group compared to the untreated group (tumor volume, 0.76 ± 0.14 *vs* 4.12 ± 0.64; and vessel volume, 0.06 ± 0.01 *vs* 0.39 ± 0.06,

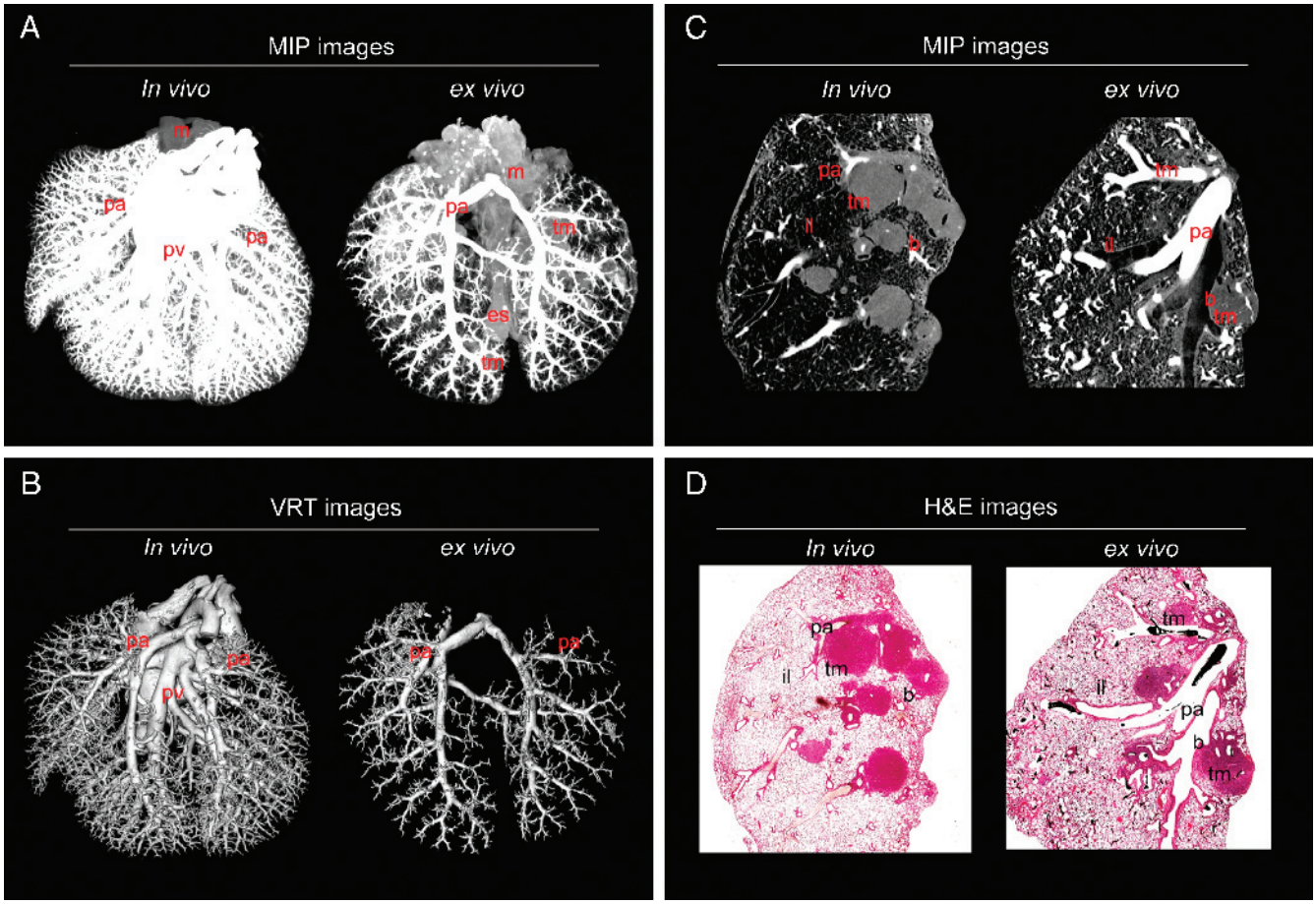

Figure 1. Micro-CT and histology of an entire murine lung after *in vivo* or *ex vivo* injection of Microfil. (A) Three-dimensional MIP images of the entire lung after *in vivo* or *ex vivo* Microfil application. (B) Three-dimensional VRT images of the entire lung after *in vivo* or *ex vivo* Microfil application. Representative micro-CT and hematoxylin and eosin–stained images clearly showed the course of anatomical structures. (C) Three-dimensional MIP images (*in vivo* or *ex vivo* Microfil application) reconstructed from micro-CT images and the corresponding (D) histologic images (*in vivo* or *ex vivo* Microfil application). *b* indicates bronchus; *es*, esophagus; *il*, inflated lung; *m*, mediasternum; *pa*, pulmonary arteries; *pv*, pulmonary veins; *tm*, tumor mass; *tr*, trachea.

respectively; Figure 3*B*). Importantly, the number of microvessels (0.0005-0.0104 mm^2 in diameter, 38,579 *vs* 18,781; 0.0905-0.1004 mm^2 in diameter, 187 *vs* 10, for untreated *vs* bevacizumab-treated, respectively) was drastically reduced with bevacizumab treatment (Figure 4*C*).

Tree analysis of tumor angiogenesis provided information on vessel structures, branching angles, and segment cross-sectional vessel area sizes. When the tree analysis or branching schematics was started at the initial seed point (~149 mm^2), in the bevacizumab-treated group, there were substantially less branching points at a smaller diameter (<25 mm^2) compared with the untreated group, confirming the anti-angiogenesis effects of bevacizumab (Figure 5, *A* and *B*).

Histomorphologic Analysis

Hematoxylin and eosin images of lung tumors of bevacizumab-treated mice showed smaller lung tumors and hemorrhage around the tumor masses compared to tumors of untreated animals (Figure 6*A*). In addition, analysis of the proliferation and vascularization of tumors derived from bevacizumab-treated and untreated tumor tissues by staining vessels with anti-vWF and assessing cell proliferation with immunohistochemical staining for the marker PCNA (Figure 6*A*). Quantitative analysis indicated a lower tumor vascular density (Figure 6*B*) and lower number of proliferating cells in bevacizumab-treated lung tumors (Figure 6*C*). Tissue density measurement by micro-CT of normal lung and lung tumor tissue in bevacizumab-treated and untreated mice with and without Microfil revealed a decrease in lung tumor tissue with contrast fluid in the treated group compared to the untreated group (Figure 6*D*), indicating that bevacizumab-treated tumor tissues were more prone to hemorrhage.

Discussion

The aim of this study was to assess the feasibility of micro-CT imaging for the quantification of lung tumor angiogenesis in Lewis lung carcinoma and adenocarcinoma mouse models. We found that micro-CT provided a detailed visualization of the vascular system of the mouse lung and lung tumors. Previous studies have described the capability of micro-CT to detect changes in organ microvasculature and its distribution pattern and connectivity [33,34]. However, this technology has not yet been used to measure mouse intrapulmonary tumors and their vascular content. When using micro-CT imaging for analysis of tumor vasculature [35], defining the binarization threshold and the scanning resolution are important methodological aspects that must be considered; we chose a binarization threshold value

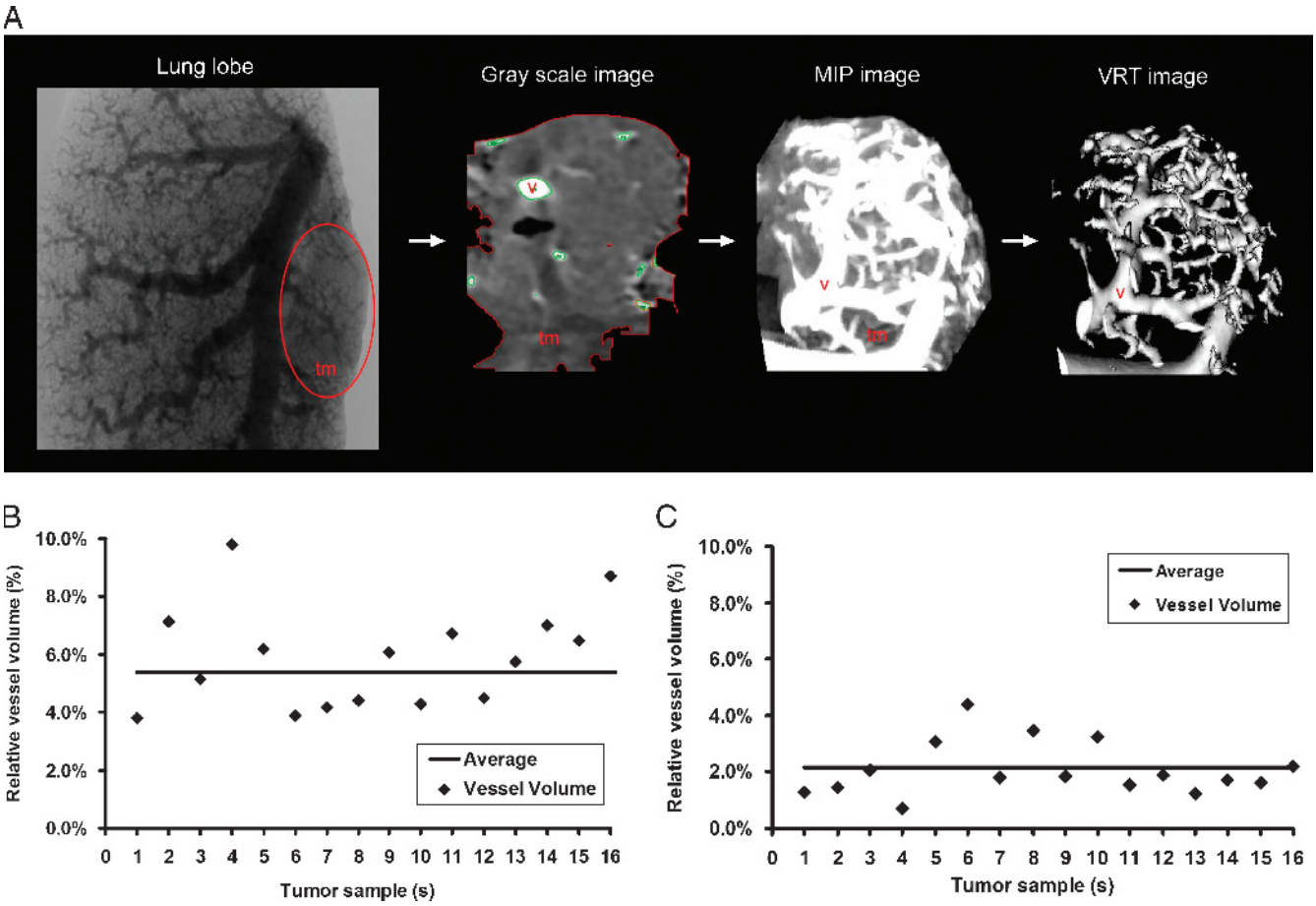

Figure 2. Quantitative volumetric measurements of extracted tumors and tumor angiogenesis after *in vivo* or *ex vivo* vessel filling. (A) A section of a Microfil-injected lung lobe: grayscale image of an extracted tumor from a Microfil-injected lung, MIP image showing a lung tumor, and a VRT image illustrating the tumor vasculature in a sequential order. Quantitative scatter graphs showing the percentage of filled vessels in tumors after *in vivo* (B) or *ex vivo* (C) Microfil application. *tm* indicates tumor mass; *v*, vessels ($n = 16$ tumors were taken for this analysis from 12 mice).

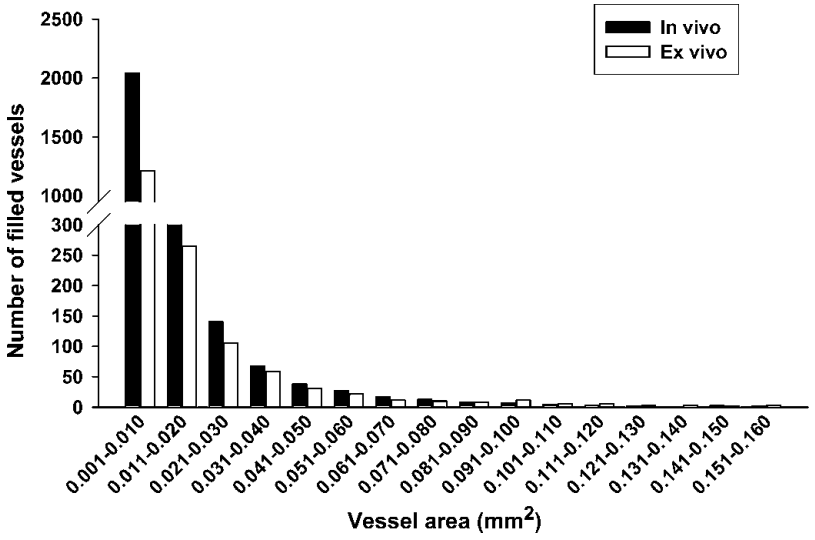

Figure 3. Quantitative measurement of tumor angiogenesis after *in vivo* or *ex vivo* vessel filling: bar graph showing the detailed information that vessels were in tumor by vessel area (mm^2; $n = 16$ tumors were taken for this analysis from 12 mice).

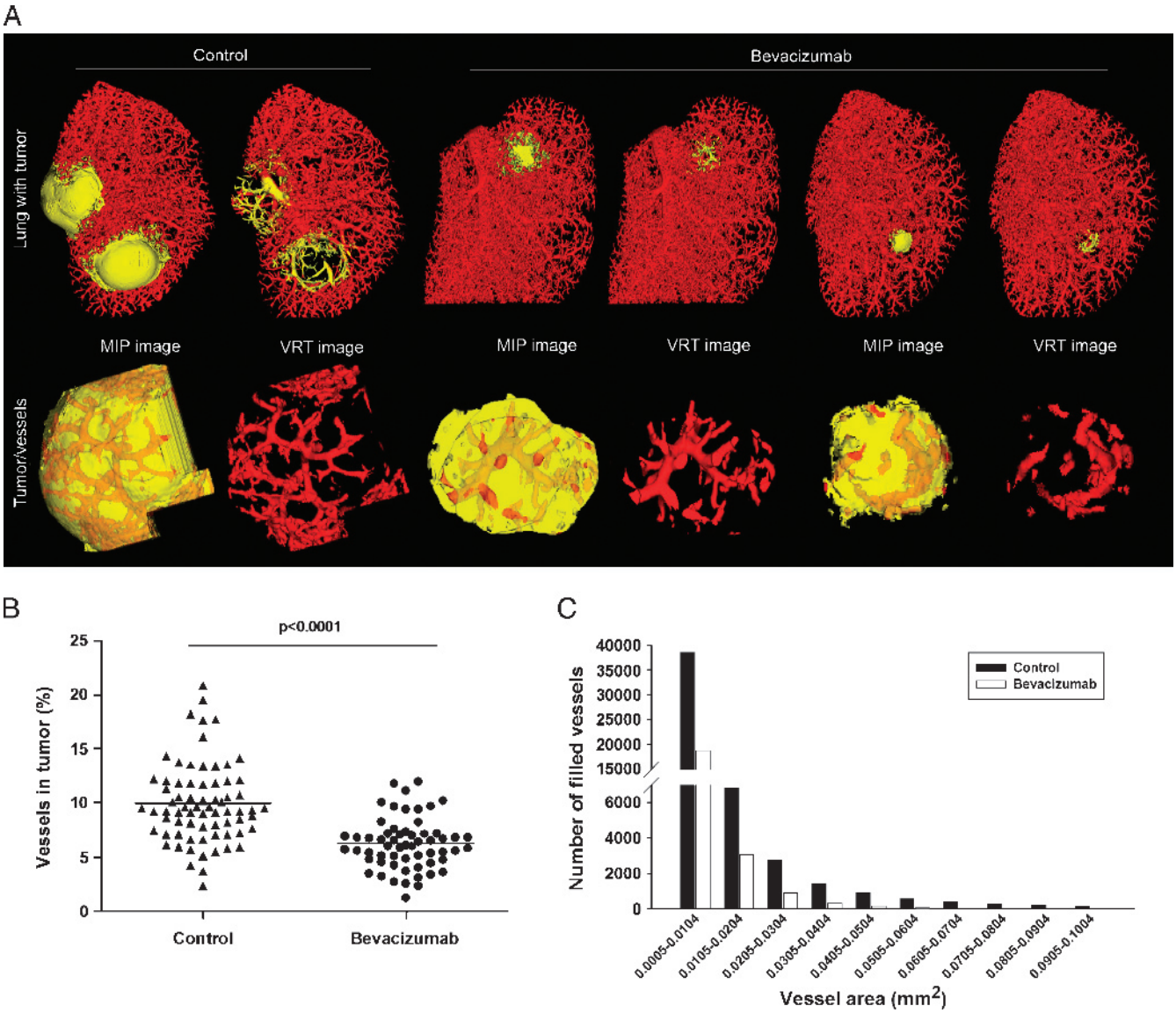

Figure 4. Measurements of tumor angiogenesis after site-specific therapy. (A) Three-dimensional surface rendering images of lung tumors from untreated and bevacizumab-treated mice. Extracted tumors and tumor microvascularization are shown (yellow represents tumor tissue area; red represents tumor vessel area). (B) Number of vessels measured with micro-CT after 14 days of bevacizumab treatment (●) or without treatment (▲). (C) Bar graph showing the detailed information that vessels were in tumor by vessel area (mm^2; n = 12 mice for each group; extracted tumors from each mouse = ~5-6).

that captured the intricate details of tumor microvasculature with minimal overestimation of broader structures. Likewise, the voxel size (6-10 μm^3) used for the scan was also selected to image smaller vascular structures [36].

In our study, although only vessels perfused with sufficient contrast material could be visualized and quantified, by using tomographic reconstruction algorithms, vessel images allowed complete stereoscopic visualization of the 3D microarchitecture of the lung tumors. As tomography allows convenient extraction of appropriate sections from 3D images, micro-CT also can be used to analyze and quantify distinct regions of interest more accurately. Furthermore, Microfil-enhanced micro-CT images (through *ex vivo* or *in vivo* filling methods) accurately depicted large-, intermediate-, and small-diameter vessels in tumors, agreed well with the corresponding histologic images (the criterion standard for tumor vessel visualization), and was useful in identifying the origin of the vessels feeding the tumors. Interestingly, *in vivo* injection of Microfil through the jugular vein filled small vessels (diameter, 0.001-0.01 mm^2) of lung tumors more efficiently than the *ex vivo* injection of Microfil through the pulmonary artery. Further, the *in vivo*–filled vessels could be tracked over long distances to their origin, allowing subsequent detection of approximately two-fold greater perfused vascular content in tumors, indicating that this method is a good choice for contrast-enhanced micro-CT for the detection of angiogenesis. The difference observed in vessel filling using the two instillation methods may be due to differences in vascular pressures. In support, the work of Molthen et al. [37] has shown that this can have a significant effect on vessel diameter and on the ability of the contrast to perfuse into small vessels (capillary pressure).

Because of its ability to generate a comprehensive display of vasculature and vessel size-specific alterations, micro-CT may be ideally suited for quantification of tumor angiogenesis and assessment of antitumor treatment effects. As our previous study demonstrated that

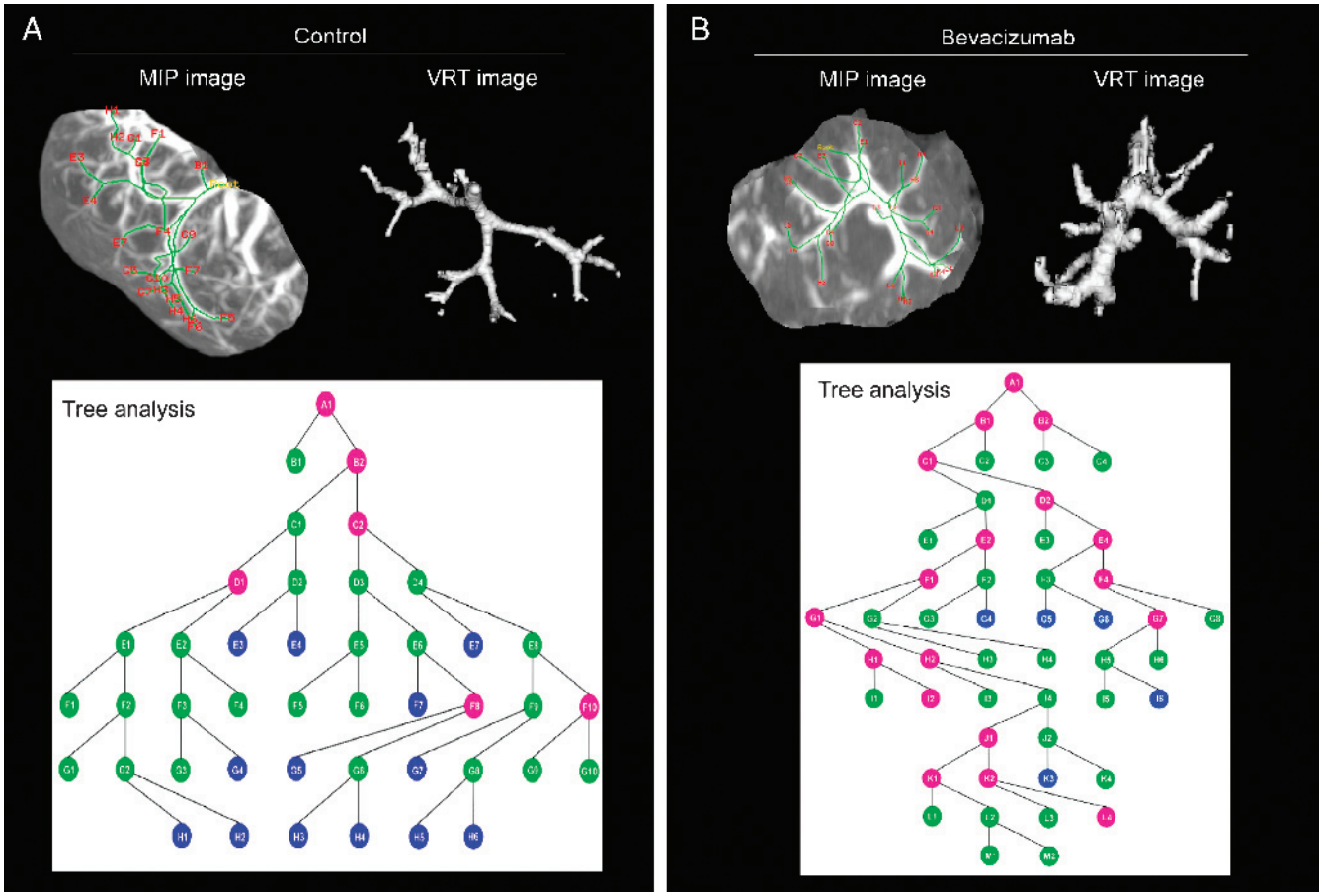

Figure 5. Lung tumor vascular branching by tree analysis: 3D MIP images, 3D VRT images, and vessel branching micrographs acquired from tree analysis of micro-CT of tumors from untreated (A) and bevacizumab-treated (B) mice. Colored circles in the branching schematics show the vessel branch points in the tumor and the vessel area: blue circles, <25 mm^2; green circles, 25 to 100 mm^2; pink circles, 100 to 150 mm^2 (n = 6 tumors were used for each group).

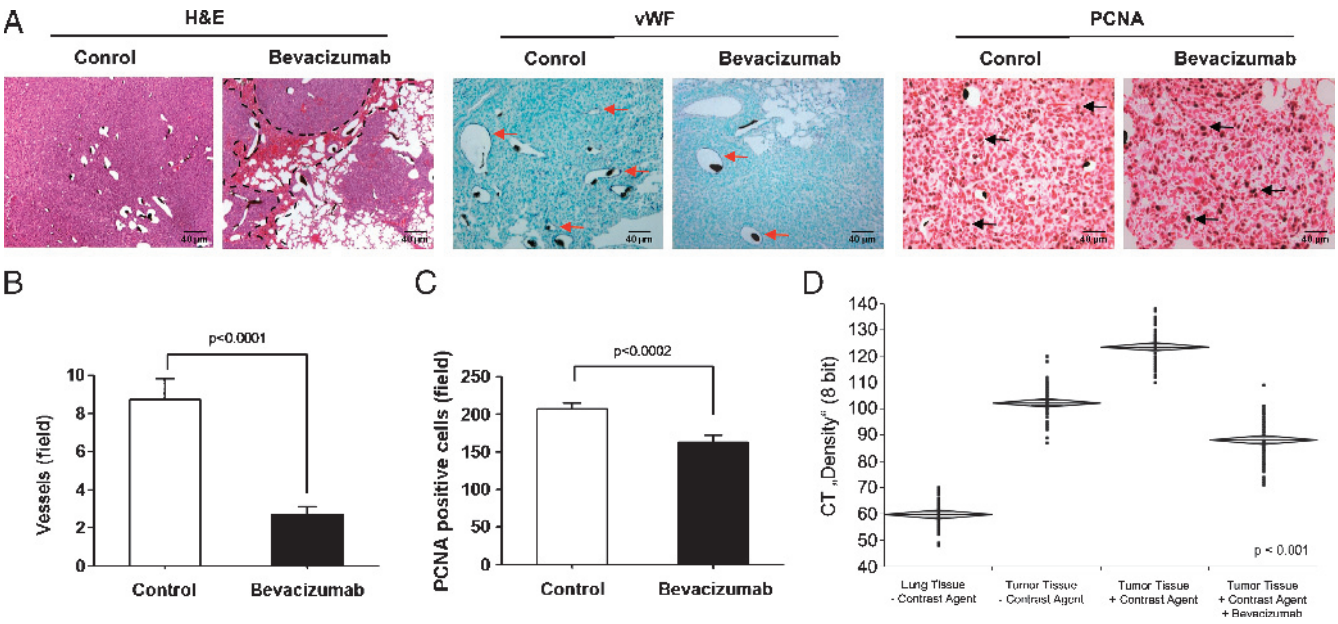

Figure 6. Histopathology of lung tumors that received bevacizumab therapy. (A) Histologic images of sections (3 μm) from untreated and bevacizumab-treated lung tumor sections that were stained with hematoxylin and eosin (H&E; the black dashed lines indicate areas of hemorrhage in the tumor), with anti-vWF (red arrows in A indicate vWF-positive vessels) and anti-PCNA (black arrows in A indicate PCNA-positive cells), respectively. Quantification of vWF-positive tumor vessels (B) and PCNA-positive tumor cells (C) by counting positively stained cells in ten randomly selected microscopic fields in seven mice is given. (D) Lung and lung tumor tissue density with or without Microfil were measured with micro-CT (60 areas were selected). Means ± SEM are shown. Scale bars, 40 μm.

the pulmonary arterial system plays an important role in the blood supply of LLC1 lung tumors [29], we implanted the A549 tumor–bearing mice with osmotic minipumps (bevacizumab-filled) through the jugular vein. This delivery mimics local delivery of antivascular agents and can be used effectively alone or in combination with cytotoxic chemotherapy for site-specific drug delivery for lung cancer treatment. As expected, continuous infusion of bevacizumab decreased lung tumor volume and tumor perfusion, with an added survival advantage compared to the untreated group. Furthermore, vessel volume and vessel area were also significantly decreased with bevacizumab treatment.

Most interestingly, our new technique allowed us to measure vessel area, and analysis of vascular tree suggested that bevacizumab treatment substantially reduced the number of small immature tumor vessels (<25 mm^2) that contribute the most to tumor nutrition. However, bevacizumab treatment had less influence on mature vessels in lung tumors, only affecting vessel dilation. These results are in line with previous studies indicating that antiangiogenic treatment has a relatively greater effect on the small/immature vasculature compared to other parts of the vasculature [38–40].

Micro-CT has several additional features compared with other techniques for tumor vessel morphologic evaluation and measurement of vessel content. Compared to histomorphometric procedures, micro-CT provides the opportunity to study the 3D connectivity of vessels and more convenient imaging of the entire organ and hence can be an alternative for quantitative measurement of intrapulmonary tumors and their vascular content in the Lewis lung carcinoma and adenocarcinoma tumor–bearing mouse models. In addition, micro-CT provides the ability to quantify the vascular parameters. Furthermore, in contrast to fpvCT, micro-CT allows the detection of immature vessels, a potential site of antiangiogenic treatment [41].

The angiogenic switch is a key event in tumor progression to a malignant, invasive, and ultimately metastasizing tumor, making angiogenesis as one of the most promising targets for novel cancer therapies. Because micro-CT, as shown in our study, can analyze tumor vascular networks in a rigorous and quantitative manner, micro-CT imaging can enhance our understanding of the impact of tumor angiogenesis and opens the possibility for future monitoring of lung cancer progression and treatment.

In conclusion, our study is the first to demonstrate micro-CT as an ideal modality to visualize the architecture of the mouse lung and lung tumor vasculature and, most importantly, to derive quantitative information from these images in LLC1 and A549 lung tumor mouse models.

An important factor in the clinical application of antiangiogenic therapy is early assessment of the therapeutic effects to predict therapy response and to allow for individualized treatment to improve outcomes. Thus, monitoring of the effects of angiogenic inhibitors on tumor vasculature has become the focus of both basic and clinical cancer researches. In this context, this study emphasizes the potential implications of vascular imaging and further expansion of new *in vivo* imaging systems for clinical cancer diagnosis and therapeutic planning.

Acknowledgments

The authors thank Gunhild Martels for excellent technical assistance with micro-CT and Kathrin Respondek for fpvCT. The authors also thank E. L. Ritman (Mayo Clinic, College of Medicine, Rochester, MN) for his critical review and comments on the manuscript.

References

[1] Jemal A, Siegel R, Ward E, Hao Y, Xu J, Murray T, and Thun MJ (2008). Cancer statistics, 2008. *CA Cancer J Clin* **58**, 71–96.

[2] Quinn MJ (2003). Cancer trends in the United States—a view from Europe. *J Natl Cancer Inst* **95**, 1258–1261.

[3] Folkman J (1990). What is the evidence that tumors are angiogenesis dependent? *J Natl Cancer Inst* **82**, 4–6.

[4] Conway EM, Collen D, and Carmeliet P (2001). Molecular mechanisms of blood vessel growth. *Cardiovasc Res* **49**, 507–521.

[5] Folkman J (2007). Angiogenesis: an organizing principle for drug discovery? *Nat Rev Drug Discov* **6**, 273–286.

[6] Ferrara N, Hillan KJ, and Novotny W (2005). Bevacizumab (Avastin), a humanized anti-VEGF monoclonal antibody for cancer therapy. *Biochem Biophys Res Commun* **333**, 328–335.

[7] Sandler A (2007). Bevacizumab in non small cell lung cancer. *Clin Cancer Res* **13**, s4613–s4616.

[8] Weidner N and Folkman J (1996). Tumoral vascularity as a prognostic factor in cancer. *Important Adv Oncol*, 167–190.

[9] Delorme S and Knopp MV (1998). Non-invasive vascular imaging: assessing tumour vascularity. *Eur Radiol* **8**, 517–527.

[10] Angeletti CA, Lucchi M, Fontanini G, Mussi A, Chella A, Ribechini A, Vignati S, and Bevilacqua G (1996). Prognostic significance of tumoral angiogenesis in completely resected late stage lung carcinoma (stage IIIA-N2). Impact of adjuvant therapies in a subset of patients at high risk of recurrence. *Cancer* **78**, 409–415.

[11] Giatromanolaki A, Sivridis E, Koukourakis MI, Polychronidis A, and Simopoulos C (2002). Prognostic role of angiogenesis in operable carcinoma of the gallbladder. *Am J Clin Oncol* **25**, 38–41.

[12] Cox G, Walker RA, Andi A, Steward WP, and O'Byrne KJ (2000). Prognostic significance of platelet and microvessel counts in operable non–small cell lung cancer. *Lung Cancer* **29**, 169–177.

[13] Ushijima C, Tsukamoto S, Yamazaki K, Yoshino I, Sugio K, and Sugimachi K (2001). High vascularity in the peripheral region of non–small cell lung cancer tissue is associated with tumor progression. *Lung Cancer* **34**, 233–241.

[14] Fanelli M, Locopo N, Gattuso D, and Gasparini G (1999). Assessment of tumor vascularization: immunohistochemical and non-invasive methods. *Int J Biol Markers* **14**, 218–231.

[15] Trivella M, Pezzella F, Pastorino U, Harris AL, and Altman DG (2007). Microvessel density as a prognostic factor in non–small-cell lung carcinoma: a meta-analysis of individual patient data. *Lancet Oncol* **8**, 488–499.

[16] Gijtenbeek JM, Wesseling P, Maass C, Burgers L, and van der Laak JA (2005). Three-dimensional reconstruction of tumor microvasculature: simultaneous visualization of multiple components in paraffin-embedded tissue. *Angiogenesis* **8**, 297–305.

[17] Guo L, Burke P, Lo SH, Gandour-Edwards R, and Lau D (2001). Quantitative analysis of angiogenesis using confocal laser scanning microscopy. *Angiogenesis* **4**, 187–191.

[18] Itoh J, Kawai K, Serizawa A, Yasumura K, Ogawa K, and Osamura RY (2000). A new approach to three-dimensional reconstructed imaging of hormone-secreting cells and their microvessel environments in rat pituitary glands by confocal laser scanning microscopy. *J Histochem Cytochem* **48**, 569–578.

[19] Hodde KC and Nowell JA (1980). SEM of micro-corrosion casts. *Scan Electron Microsc* **pt 2**, 89–106.

[20] Bentley MD, Ortiz MC, Ritman EL, and Romero JC (2002). The use of microcomputed tomography to study microvasculature in small rodents. *Am J Physiol Regul Integr Comp Physiol* **282**, R1267–R1279.

[21] Ritman EL (2002). Molecular imaging in small animals—roles for micro-CT. *J Cell Biochem Suppl* **39**, 116–124.

[22] Jorgensen SM, Demirkaya O, and Ritman EL (1998). Three-dimensional imaging of vasculature and parenchyma in intact rodent organs with x-ray micro-CT. *Am J Physiol* **275**, H1103–H1114.

[23] Lerman A and Ritman EL (1999). Evaluation of microvascular anatomy by micro-CT. *Herz* **24**, 531–533.

[24] Garcia-Sanz A, Rodriguez-Barbero A, Bentley MD, Ritman EL, and Romero JC (1998). Three-dimensional microcomputed tomography of renal vasculature in rats. *Hypertension* **31**, 440–444.

[25] Ortiz MC, Garcia-Sanz A, Bentley MD, Fortepiani LA, Garcia-Estan J, Ritman EL, Romero JC, and Juncos LA (2000). Microcomputed tomography of kidneys following chronic bile duct ligation. *Kidney Int* **58**, 1632–1640.

[26] Wan SY, Kiraly AP, Ritman EL, and Higgins WE (2000). Extraction of the hepatic vasculature in rats using 3-D micro-CT images. *IEEE Trans Med Imaging* **19**, 964–971.

[27] Rodriguez-Porcel M, Lerman A, Ritman EL, Wilson SH, Best PJ, and Lerman LO (2000). Altered myocardial microvascular 3D architecture in experimental hypercholesterolemia. *Circulation* **102**, 2028–2030.

[28] Pistoia W, van Rietbergen B, Laib A, and Ruegsegger P (2001). High-resolution three-dimensional–pQCT images can be an adequate basis for *in-vivo* microFE analysis of bone. *J Biomech Eng* **123**, 176–183.

[29] Savai R, Wolf JC, Greschus S, Eul BG, Schermuly RT, Hanze J, Voswinckel R, Langheinrich AC, Grimminger F, Traupe H, et al. (2005). Analysis of tumor vessel supply in Lewis lung carcinoma in mice by fluorescent microsphere distribution and imaging with micro- and flat-panel computed tomography. *Am J Pathol* **167**, 937–946.

[30] Greschus S, Savai R, Wolf JC, Rose F, Seeger W, Fitzgerald P, and Traupe H (2007). Non-invasive screening of lung nodules in mice comparing a novel volumetric computed tomography with a clinical multislice CT. *Oncol Rep* **17**, 707–712.

[31] Fluiter K, Ten Asbroek AL, van Groenigen M, Nooij M, Aalders MC, and Baas F (2002). Tumor genotype–specific growth inhibition *in vivo* by antisense oligonucleotides against a polymorphic site of the large subunit of human RNA polymerase II. *Cancer Res* **62**, 2024–2028.

[32] Langheinrich AC, Bohle RM, Greschus S, Hackstein N, Walker G, Von GS, Rau WS, and Holschermann H (2004). Atherosclerotic lesions at micro CT: feasibility for analysis of coronary artery wall in autopsy specimens. *Radiology* **231**, 675–681.

[33] Duvall CL, Taylor WR, Weiss D, and Guldberg RE (2004). Quantitative microcomputed tomography analysis of collateral vessel development after ischemic injury. *Am J Physiol Heart Circ Physiol* **287**, H302–H310.

[34] Rodriguez-Porcel M, Zhu XY, Chade AR, Amores-Arriaga B, Caplice NM, Ritman EL, Lerman A, and Lerman LO (2006). Functional and structural remodeling of the myocardial microvasculature in early experimental hypertension. *Am J Physiol Heart Circ Physiol* **290**, H978–H984.

[35] Luo G, Kinney JH, Kaufman JJ, Haupt D, Chiabrera A, and Siffert RS (1999). Relationship between plain radiographic patterns and three-dimensional trabecular architecture in the human calcaneus. *Osteoporos Int* **9**, 339–345.

[36] Maehara N (2003). Experimental microcomputed tomography study of the 3D microangioarchitecture of tumors. *Eur Radiol* **13**, 1559–1565.

[37] Molthen RC, Karau KL, and Dawson CA (2004). Quantitative models of the rat pulmonary arterial tree morphometry applied to hypoxia-induced arterial remodeling. *J Appl Physiol* **97**, 2372–2384.

[38] Benjamin LE, Golijanin D, Itin A, Pode D, and Keshet E (1999). Selective ablation of immature blood vessels in established human tumors follows vascular endothelial growth factor withdrawal. *J Clin Invest* **103**, 159–165.

[39] Jain RK (2001). Normalizing tumor vasculature with anti-angiogenic therapy: a new paradigm for combination therapy. *Nat Med* **7**, 987–989.

[40] Gee MS, Procopio WN, Makonnen S, Feldman MD, Yeilding NM, and Lee WM (2003). Tumor vessel development and maturation impose limits on the effectiveness of anti-vascular therapy. *Am J Pathol* **162**, 183–193.

[41] Kiessling F, Greschus S, Lichy MP, Bock M, Fink C, Vosseler S, Moll J, Mueller MM, Fusenig NE, Traupe H, et al. (2004). Volumetric computed tomography (VCT): a new technology for noninvasive, high-resolution monitoring of tumor angiogenesis. *Nat Med* **10**, 1133–1138.